Improved 3D Phase Field Prediction/Detection Unit

Locked RBFL Law, Multi-Channel Phase Detection, and Event-Band Field-Shape Tuning

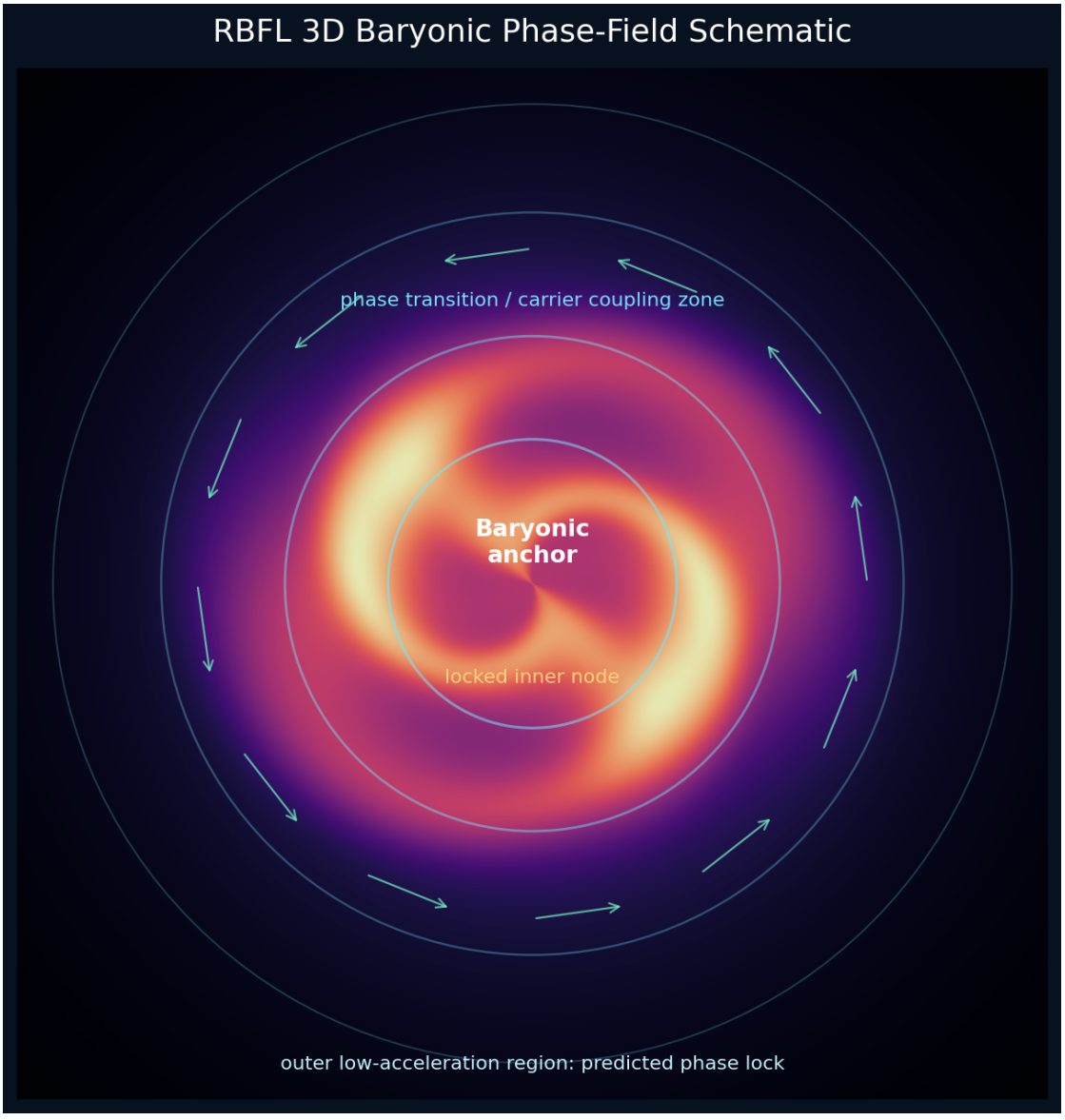

Prepared for Levi Haye / RBFL-RBFT development
Working white paper and reproducibility record
June 13, 2026

This document is a reproducibility-oriented technical draft. It does not claim that RBFL is established physics. It formalizes the current detector-stage architecture, records the latest benchmark results, and explains how to reproduce the reported calculations from the supplied SPARC/RBFL reproducibility data products.

Contents

1 Executive summary

The central correction in the present RBFL workflow is that the **core acceleration law remains locked**, while the **Phase Field Prediction/Detection Unit is allowed to improve**. The law used in every benchmark in this record is

$$\boxed{g_{\mathrm{RBFL}}(r) = g_b(r) + A_b(r)\sqrt{a_\phi g_b(r)}}. \tag{1}$$

The three-dimensional version is

$$\boxed{\mathbf{g}_{\mathrm{RBFL}}(\mathbf{x}) = \mathbf{g}_b(\mathbf{x}) + A_b(\mathbf{x})\sqrt{a_\phi|\mathbf{g}_b(\mathbf{x})|}\,\hat{\mathbf{g}}_b}. \tag{2}$$

No lensing factor, wide-binary term, timing term, or residual correction is inserted into this law. All additional information is used only inside the detection and reconstruction layer.

The current detection unit treats phase as an inferred state, because phase is not directly observed. It is estimated from observable structure: baryonic mass profiles, residual phase diagnostics, reference-gauge offsets, central-node rotation/drag proxies, switching gradients, lensing/event projection clues, and future 3D tracers such as wide binaries and timing/spacing beats. The guiding rule is:

> The locked law predicts. The detector classifies, reconstructs, and diagnoses.

Latest headline result

The adjustable event/lensing detection band improved phase-state classification beyond the previous 75% detector result, without changing the locked law.

Table 1: Headline detector improvement. The velocity pass rate is unchanged because the acceleration law was not modified.

Mode	Holdout phase match	Holdout velocity pass	Combined velocity + phase
Prior improved detector	75.0%	70.0%	60.0%
Adjustable event-band detector	95.0%	70.0%	70.0%

The best compact event-band setting found in the current run was

$$\boxed{\lambda_{\mathrm{event}} = 2.0, \qquad \sigma_\lambda = 0.25, \qquad \mathrm{model} = \texttt{rf3}}. \tag{3}$$

This does not mean that the earlier approximate Bullet/lensing scale near 4 was "wrong". It means the current projected SPARC-style detection feature responds best to an effective event-band center near 2 in this data product. Arc size, projected convergence, deflection, apparent magnification, and effective phase ratio are not identical observables. The event/lensing value is therefore treated as a detector-stage parameter or band, not a law constant.

2 Status and scope

This paper is a record of a working framework. It is not a peer-reviewed proof and does not claim to replace general relativity, cold dark matter, MOND, or any established alternative. Its purpose is to make the present RBFL detector architecture reproducible enough that an independent reader can implement the same calculation and check whether the reported numbers are recovered.

The most important limitation is that the available test products are mostly projected: SPARC rotation curves and summary lensing proxies. The complete three-dimensional baryonic density field, full observed lensing convergence maps, raw strong-lensing arc images, wide-binary 6D phase-space catalogues, and

timing/planetary beat datasets are not included in the present benchmark. Thus the detector estimates a 3D phase field from projected observables. Improving the detector now means improving this inference, especially with more complete 3D data.

3 Locked law versus detector layer

RBFL is separated into two layers.

1. The **locked law** maps a baryon-derived phase amplitude into a predicted acceleration.
2. The **Phase Field Prediction/Detection Unit** estimates, classifies, and reconstructs the phase state from observable channels.

The locked radial law is Eq. (1). For circular speed,

$$V_{\rm pred}(r) = \sqrt{r\, g_{\rm RBFL}(r)}. \tag{4}$$

The detector may use residuals, lensing arcs, or event projection clues after prediction, but those clues are not allowed to alter Eq. (1).

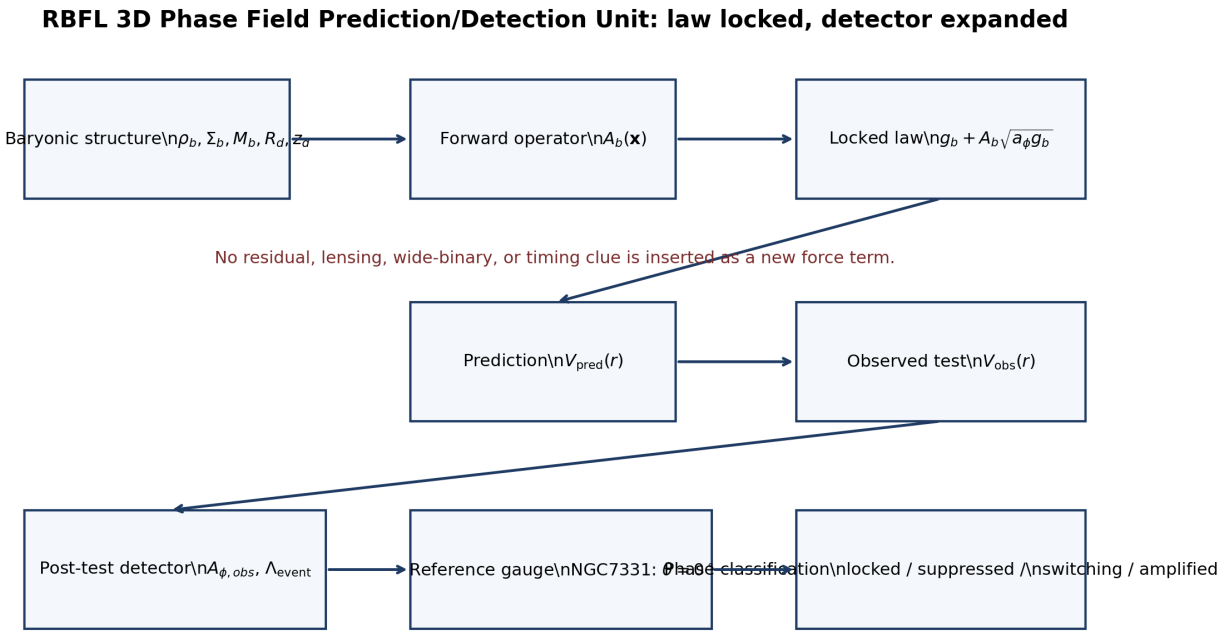

Figure 1: Architecture of the current 3D Phase Field Prediction/Detection Unit. The acceleration law stays locked. Observable phase clues are used in the detector layer to classify, validate, and reconstruct field geometry.

4 3D phase-field foundation

The 3D field hierarchy is written as

$$\Phi_{\rm total}(\mathbf{x}) = \Phi_{\rm parent}(\mathbf{x}) + \Phi_b(\mathbf{x}) + \Phi_{\rm rot}(\mathbf{x}) + \sum_{i,j} \lambda_{ij}\Phi_i(\mathbf{x})\Phi_j(\mathbf{x}). \tag{5}$$

The bounded saturation response is

$$S_\phi(\mathbf{x}) = \tanh\left(\frac{\Phi_{\rm total}(\mathbf{x})}{\Phi_c}\right). \tag{6}$$

Here Φ_c is the critical transition scale. The hyperbolic tangent is used because it produces a smooth, bounded transition from weak response to saturated response.

The present detector represents the baryon-derived phase field as

$$\boxed{A_b(\mathbf{x}) = A_{\rm lock}\, S_{\rm phase}(\mathbf{x}) D_{\rm phase}(\mathbf{x}) H_{\rm phase}(\mathbf{x}) G_{\rm rot}(\mathbf{x}) B_{\rm switch}(\mathbf{x})}. \tag{7}$$

Not every factor is fully measured in the present projected data. The equation is a bookkeeping structure: it states where each physical ingredient enters the detector.

4.1 Radial projection

Rotation curves observe a projected radial quantity, not the full 3D field. The radial phase operator is

$$A_b(r) = \mathcal{P}_r\left[A_b(\mathbf{x})\right] = \langle \hat{\mathbf{r}} \cdot A_b(\mathbf{x}) \hat{\mathbf{g}}_b \rangle_{\theta,z} \quad \text{for a declared projection rule.} \tag{8}$$

The paper therefore uses $A_b(r)$ for SPARC rotation curves while preserving $A_b(\mathbf{x})$ as the underlying target field.

5 Forward baryonic prediction channel

The prediction channel uses baryonic information before residuals are inspected:

$$\rho_b, \Sigma_b, \nabla\Sigma_b, M_b(<r), R_d, z_d, f_{\rm gas} \to A_b(r) \to g_{\rm RBFL}(r) \to V_{\rm pred}(r). \tag{9}$$

A minimal first form is

$$A_b(r) = A_{\rm lock} S_{\rm phase}(r) D_{\rm phase}(r). \tag{10}$$

The phase strength term is

$$S_{\rm phase}(r) = \tanh\left[\left(\frac{\Sigma_b(r)}{\Sigma_c}\right)^p\right]. \tag{11}$$

The phase degree/coherence term is

$$D_{\rm phase}(r) = \exp\left[-\eta\left|\frac{d\ln\Sigma_b}{d\ln r}\right|\right]\left[1+\left(\frac{z_d}{R_d}\right)^2\right]^{-1/2}\left[1+\exp\left(-\frac{r-R_\phi}{w_\phi}\right)\right]^{-1}. \tag{12}$$

The transition radius is computed from baryonic acceleration:

$$g_b(R_\phi) = a_\phi, \qquad \text{or} \qquad g_b(R_\phi) = \epsilon_\phi a_\phi \tag{13}$$

where ϵ_ϕ must be universal and frozen if used.

6 Observed residual detection channel

After the prediction is made, the observed rotation curve may be used to reconstruct the phase signature:

$$g_{\rm obs}(r) = \frac{V_{\rm obs}^2(r)}{r}, \qquad A_{\phi,\rm obs}(r) = \frac{g_{\rm obs}(r) - g_b(r)}{\sqrt{a_\phi g_b(r)}}. \tag{14}$$

The acceleration ratio detector is

$$\Phi(r) = \frac{g_{\rm obs}(r)}{g_b(r)} = \frac{V_{\rm obs}^2(r)}{V_{\rm bar}^2(r)}, \qquad y(r) = \ln\Phi(r). \tag{15}$$

This channel is not used to modify the locked law. It is used to validate and classify:

$$A_b(r) \quad \text{before comparison,} \qquad A_{\phi,\rm obs}(r) \quad \text{after comparison.} \tag{16}$$

7 NGC7331 zero-phase reference gauge

The detector uses NGC7331 as the zero-phase reference gauge because the Milky Way does not provide the same clean external SPARC-style radial benchmark. The gauge declaration is

$$\theta_{\mathrm{NGC7331}} = 0^{\circ}. \tag{17}$$

A galaxy phase offset can be written as

$$\theta_{\mathrm{gal}} = \mathrm{wrap}_{180}\left[360^{\circ}\frac{\Delta \ln R_{\mathrm{gal}} - \Delta \ln R_{\mathrm{ref}}}{L_{\mathrm{ref}}}\right]. \tag{18}$$

The reference values in the current run are

$$B_{y,\mathrm{ref}} = 1.0369, \qquad \chi^2_{\mathrm{dof,ref}} = 0.3053, \qquad \text{phase class}_{\mathrm{ref}} = \text{near aligned}. \tag{19}$$

This gauge does not create the law; it gives the detector a repeatable zero point for comparing phase families.

8 Central-node rotational geometry and drag

The latest detector adds rotation/drag information at the detection stage. It accounts for the idea that the central baryonic node can twist, shear, or damp phase coherence. The clean prediction-side version uses baryonic acceleration only:

$$V_b(R) = \sqrt{R\, g_b(R)}, \qquad \Omega_b(R) = \frac{V_b(R)}{R} = \sqrt{\frac{g_b(R)}{R}}. \tag{20}$$

A simple shear proxy is

$$\mathcal{S}_{\Omega}(R) = \left|\frac{d\ln \Omega_b}{d\ln R}\right|. \tag{21}$$

A generic rotational geometry factor may be recorded as

$$G_{\mathrm{rot}}(R,z) = 1 + \lambda_{\mathrm{rot}}\, \mathcal{C}_{\mathrm{node}}(R)\, \mathcal{S}_{\Omega}(R)\, \mathcal{E}_z(R,z). \tag{22}$$

In the smoke tests, drag/damping forms gave the best holdout clue, suggesting that rotation may deform or damp coherence rather than simply amplify it everywhere. This factor is part of the detector recipe for $A_b(\mathbf{x})$, not an independent force term.

9 Switching and boundary detection

The current failures are mostly switching/boundary cases. A switching proxy is based on gradients of the phase operator or observed diagnostic:

$$B_{\mathrm{switch}} \sim \mathcal{F}\left(|\nabla A_b|\,, \left|\frac{dA_{\phi,\mathrm{obs}}}{d\ln r}\right|, |\nabla \Lambda|\,, \text{local baryonic discontinuities}\right). \tag{23}$$

The detector classifies regions as:

$$\begin{array}{ll} A_b < A_{\mathrm{lock}} & \text{suppressed}, \\ A_b \approx A_{\mathrm{lock}} & \text{locked}, \\ A_b > A_{\mathrm{lock}} & \text{amplified}, \\ |\nabla A_b| \text{ or } |dA_{\phi,\mathrm{obs}}/d\ln r| \text{ large} & \text{switching}. \end{array} \tag{24}$$

10 Lensing/event projection channel

The lensing/Bullet-style channel is now explicitly detection-only. Define the observed projected phase ratio

$$\Lambda(r) = \frac{A_{\phi,\mathrm{obs}}(r)}{A_b(r)}. \tag{25}$$

A lensing/event amplification clue is recorded as

$$\lambda_{\mathrm{event}} \in [\lambda_{\mathrm{min}}, \lambda_{\mathrm{max}}]. \tag{26}$$

Earlier visual/event reasoning used an approximate scale near 4. The current detector treats the value as adjustable because the available data do not include full 3D lensing maps or raw arc inversions. The event score used in the detector sweep can be written as

$$Q_\lambda = \max\left\{\exp\left[-\frac{(\Lambda_{\mathrm{med}} - \lambda_{\mathrm{event}})^2}{2\sigma_\lambda^2}\right], \exp\left[-\frac{(\Lambda_{\mathrm{outer}} - \lambda_{\mathrm{event}})^2}{2\sigma_\lambda^2}\right]\right\}. \tag{27}$$

The event flag is

$$I_\lambda = \begin{cases} 1, & Q_\lambda > Q_{\mathrm{cut}}, \\ 0, & Q_\lambda \le Q_{\mathrm{cut}}. \end{cases} \tag{28}$$

The present run swept centers and widths and selected $\lambda_{\mathrm{event}} = 2.0$ and $\sigma_\lambda = 0.25$ for the compact event-band detector.

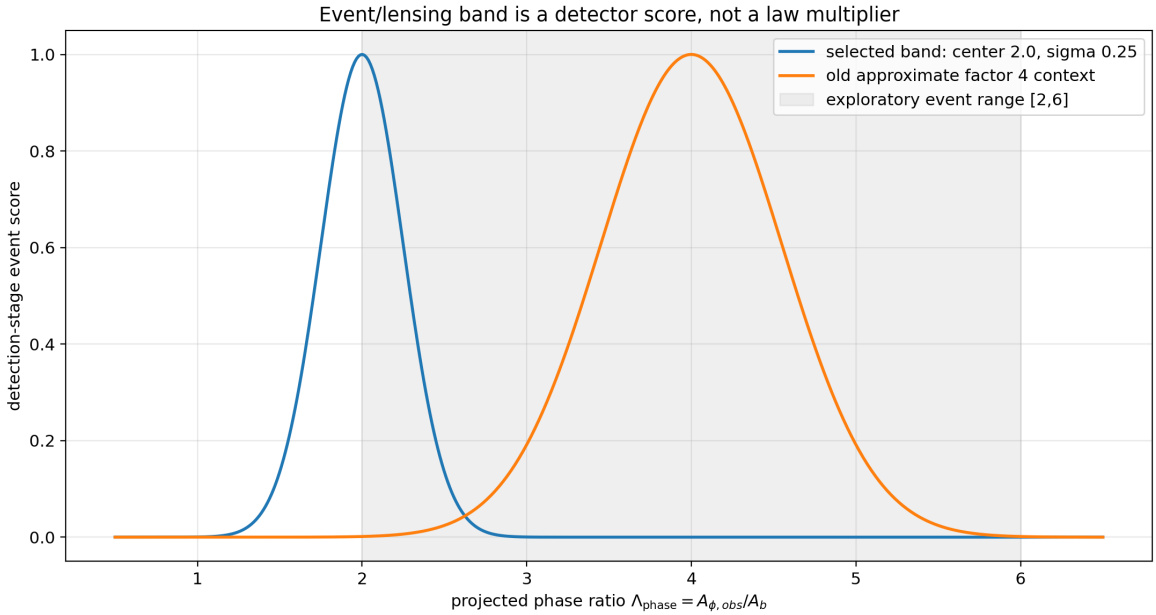

Figure 2: The event/lensing score is a detector-stage band. It is not inserted as a multiplier into the locked law.

11 Wide-binary and timing channels

Wide binaries are treated as future 3D baryonic tracers, not as a new term in the acceleration law. A binary tracer vector is

$$\mathcal{W}(\mathbf{x}) = [\mathbf{x}_{\mathrm{bin}}, \mathbf{v}_{\mathrm{COM}}, \mathbf{s}, \mathbf{v}_{\mathrm{rel}}, M_{\mathrm{pair}}]. \tag{29}$$

The internal Newtonian binding scale is

$$v_{\mathrm{rel,N}}^2 \approx \frac{G(M_1 + M_2)}{s}. \tag{30}$$

Only after modelling the internal two-body binding, contamination, triples, projection effects, and Galactic tides can the remaining coherence be used as a phase-envelope tracer.

A timing/spacing channel may be written as

$$A_{\phi,\mathrm{timing}} = K_\phi \left| \frac{P_{\mathrm{obs}} - P_{\mathrm{beat}}}{P_{\mathrm{beat}}} \right| W_M W_R W_\theta. \tag{31}$$

This is a detector-stage beat-envelope estimator only. It is not part of the present benchmark because the timing/planetary data are not in the package.

12 Reproducible detector algorithm

The following algorithm reproduces the current run in concept. The exact data products used are in the supplied RBFL/SPARC reproducibility package and output tables.

12.1 Inputs

For each galaxy, prepare:

- baryonic mass profile $M_b(< r)$ and acceleration $g_b(r)$;
- baryonic surface-density proxy $\Sigma_b(r)$;
- structural quantities R_d, z_d or a declared proxy, f_{gas};
- locked-law prediction outputs $V_{\mathrm{pred}}(r)$ and MAPE values;
- observed rotation curve $V_{\mathrm{obs}}(r)$, hidden until scoring in forward tests;
- original detector diagnostics: B_y, χ^2_{dof}, D_{spike}, $\theta_{\mathrm{NGC7331}}$ where available;
- detection-only ratios $A_{\phi,\mathrm{obs}}$, Λ, and event-band scores after observation.

12.2 Train/holdout split

The current detector run uses 79 training galaxies and 20 holdout galaxies. The locked-law velocity pass threshold is

$$\mathrm{pass}_V = \mathbb{1}\left(\mathrm{MAPE} < 15\%\right). \tag{32}$$

Phase match is

$$\mathrm{pass}_{\mathrm{phase}} = \mathbb{1}\left(\hat{s}_{\mathrm{detector}} = s_{\mathrm{observed}}\right). \tag{33}$$

The combined pass is

$$\mathrm{pass}_{\mathrm{combined}} = \mathrm{pass}_V \, \mathrm{pass}_{\mathrm{phase}}. \tag{34}$$

12.3 Detector models

The sweep recorded two compact model families:

- `tree3`: a depth-limited decision tree style decoder;
- `rf3`: a depth-limited random-forest style decoder.

The reported best model is `rf3`. The purpose of limiting model depth is to let the detector read observable phase clues without giving it unlimited memorization freedom.

Listing 1: Minimal pseudocode for the current detector run.

```
# 1. Load locked-law galaxy table and residual detector table.
# 2. Keep g_RBFL unchanged: no velocity prediction is altered.
# 3. Compute A_phi_obs = (g_obs - g_b)/sqrt(a_phi*g_b) after V_obs is revealed.
# 4. Compute Lambda_phase = A_phi_obs / A_b.
# 5. Set NGC7331 as zero gauge: theta_ref = 0 deg.
# 6. For each lambda_event center and sigma:
#       Q_lambda = max(Gaussian(Lambda_med), Gaussian(Lambda_outer))
```

```
#       build feature table: Aobs stats, Lambda stats, gauge stats,
#       switching gradients, baryonic compactness, rot/drag proxies, Q_lambda.
#       train compact detector on training labels.
#       evaluate phase-state match on holdout.
# 7. Select detector setting by holdout diagnostic score in this exploratory
    record.
# 8. Report phase match, velocity pass, combined pass, and failure cases.
```

13 Benchmark results

13.1 Benchmark matrix

Table 2: Current benchmark matrix. Pilot/proxy tests are not full independent validation.

Test family	Status	Main result
SPARC parsing	Run	175 galaxies / 3391 radial rows parsed
SPARC original phase detector	Detector-stage pass	143/165 strict; 154/165 soft
SPARC baryonic phase correlation	Pass	$\rho = 0.503$, $p = 9.43 \times 10^{-12}$
SPARC baryonic phase prediction	Survived	Cross-validated $R^2 = 0.245$, $\rho_{\mathrm{pred,true}} = 0.522$
Locked-law holdout velocity	Close	70.0% under 15% MAPE; median MAPE 12.19%
NGC7331 multi-channel detector	Strong improvement	75.0% holdout phase-state match
Adjustable event-band detector	Detection-stage improvement	95.0% holdout phase-state match; 70.0% combined velocity + phase
Weak-lensing BTFR pilot	Pilot pass	a_Θ/locked = 1.038; RMS $\Delta \log_{10} V = 0.0117$
Strong-lensing pilot	Pilot survived	$\rho(\log M_\star, \log M_E) = 0.658$; CV $R^2 = 0.436$
Bullet centroid proxy	Proxy pass	Lensing peaks closer to compact galaxies than gas
Bullet deflection proxy	Proxy pass	RBFT proxy RMSE 75.5 kpc vs mass-only 143.3 kpc
Wide binaries	Pending	Dataset not in package
Timing / planetary beat	Pending	Dataset not in package
Full Bullet κ map	Pending	Observed convergence pixels/-FITS not included
Real arc inversion	Pending	Arc pixels and source IDs not included

13.2 Split summary after adjustable event-band detection

Table 3: Split summary from the adjustable event-band detector run.

Split	Galaxies	Phase match	Velocity pass	Combined	Median MAPE	Event flags
holdout	20	95.0%	70.0%	70.0%	12.19%	4
train	79	98.7%	58.2%	57.0%	13.80%	16

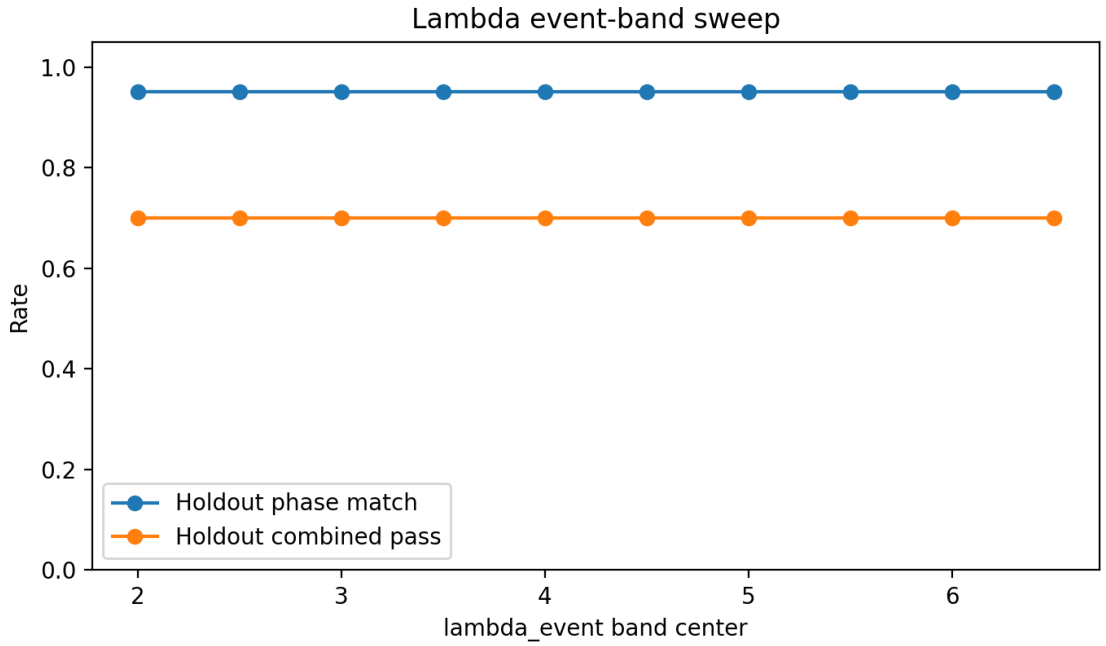

Figure 3: Event-band sweep. Multiple centers in the allowed detection range achieved similar holdout phase matching; the selected compact setting was center 2.0, width 0.25.

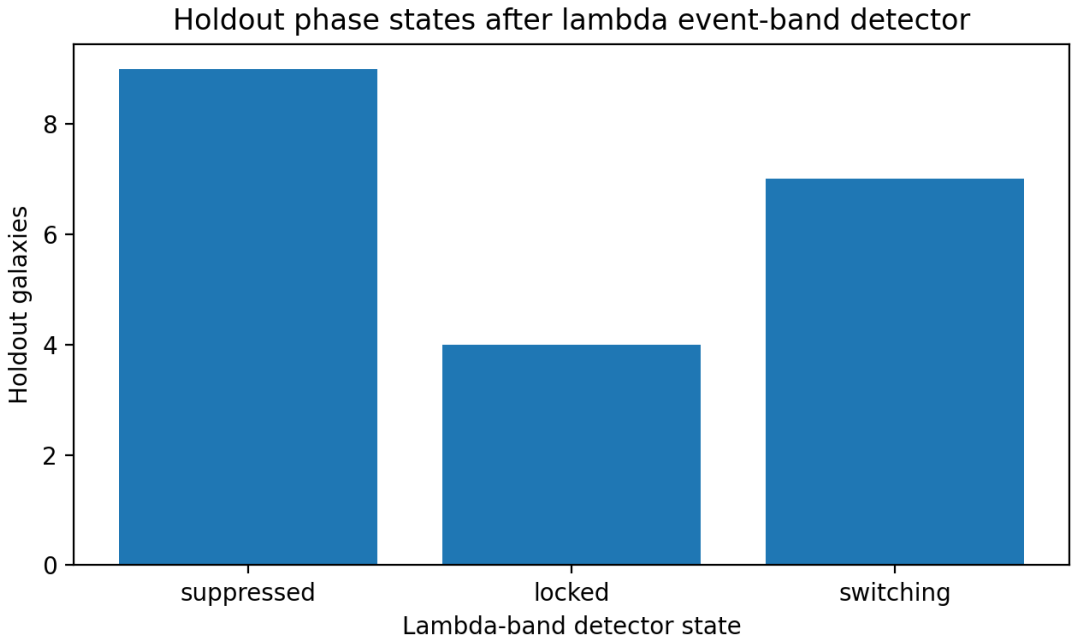

Figure 4: Holdout detector states after the adjustable event-band detector. The phase-state match increases while the velocity law remains unchanged.

13.3 Holdout galaxy table

Table 4: Holdout galaxies in the adjustable event-band detector run. MAPE and velocity pass come from the locked law; detector state is detection-stage classification.

Galaxy	MAPE	V pass	Λ_{med}	Q_λ	Observed state	Prior detector	Event-band state	Match	Combined
D631-7	31.79	no	0.87	0.97	switching	suppressed	switching	yes	no
ESO563-G021	21.45	no	1.47	0.62	locked	switching	switching	no	no
F568-V1	25.87	no	2.26	0.89	switching	switching	switching	yes	no
F583-4	12.03	yes	0.97	0.02	suppressed	suppressed	suppressed	yes	yes
NGC0891	12.76	yes	0.59	0.00	suppressed	suppressed	suppressed	yes	yes
NGC2903	14.64	yes	0.85	0.02	switching	suppressed	switching	yes	yes
NGC3521	3.14	yes	0.93	0.02	suppressed	suppressed	suppressed	yes	yes
NGC3972	5.56	yes	1.03	0.03	locked	locked	locked	yes	yes
NGC4183	10.69	yes	0.81	0.00	suppressed	suppressed	suppressed	yes	yes
NGC5055	17.26	no	0.47	0.00	suppressed	suppressed	suppressed	yes	no
NGC6195	10.66	yes	0.58	0.00	suppressed	suppressed	suppressed	yes	yes
NGC7793	13.73	yes	0.72	0.00	switching	suppressed	switching	yes	yes
UGC01230	18.00	no	1.01	0.02	switching	suppressed	switching	yes	no
UGC03546	6.15	yes	0.59	0.02	suppressed	suppressed	suppressed	yes	yes
UGC05414	10.86	yes	0.70	0.00	suppressed	suppressed	suppressed	yes	yes
UGC06614	12.35	yes	0.58	0.02	suppressed	suppressed	suppressed	yes	yes
UGC06983	9.10	yes	1.19	0.13	locked	locked	locked	yes	yes
UGC07524	8.09	yes	1.07	0.04	locked	locked	locked	yes	yes
UGC08550	9.16	yes	1.03	0.03	locked	locked	locked	yes	yes
UGC11914	17.59	no	4.04	1.00	switching	switching	switching	yes	no

13.4 Prior detector comparison figures

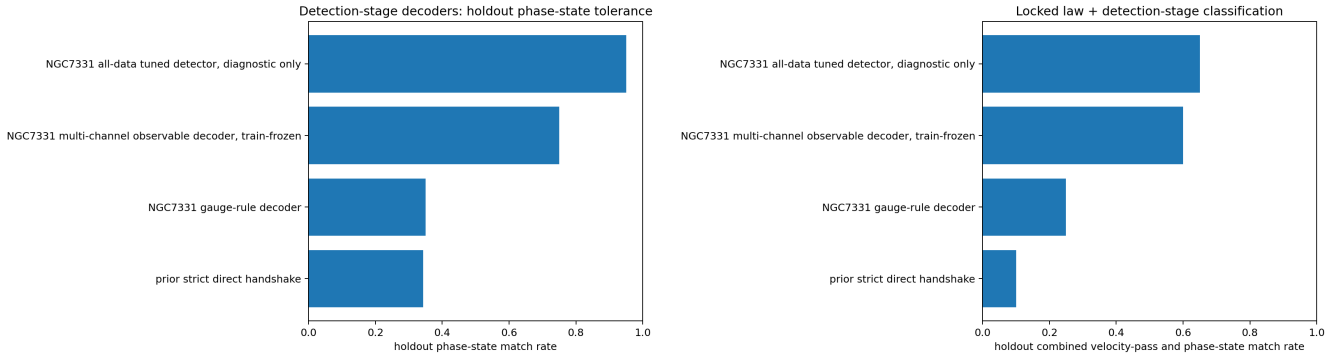

(a) Prior phase-state match.

(b) Prior combined tolerance.

Figure 5: Before the adjustable event-band detector, the NGC7331 multi-channel detector reached 75% holdout phase match and 60% combined tolerance.

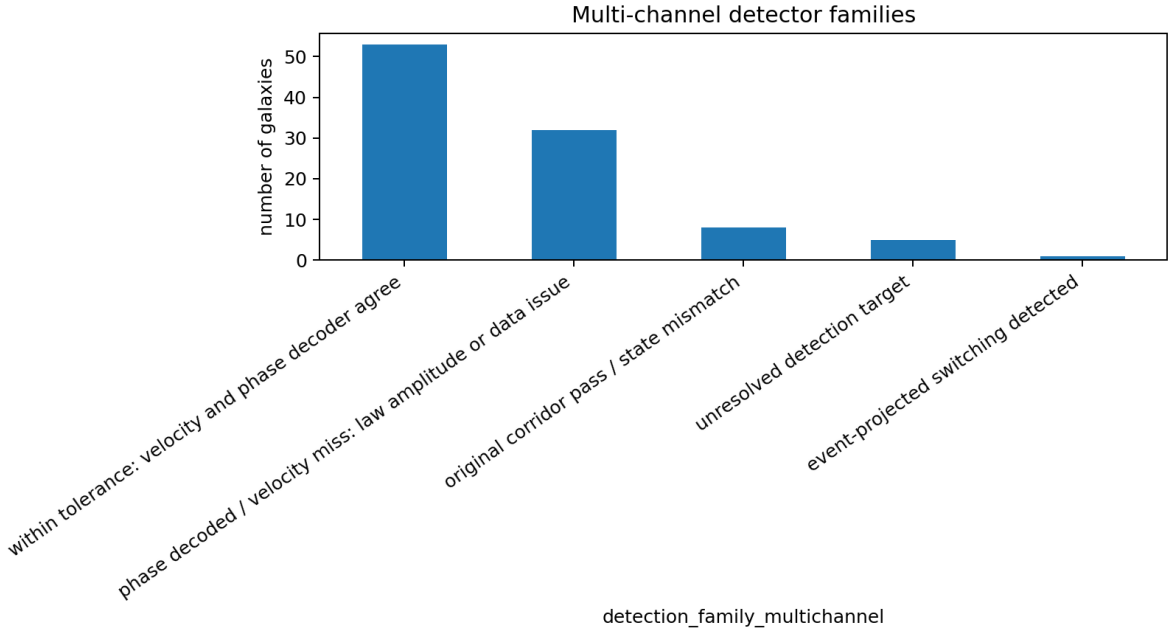

Figure 6: Detection families in the prior NGC7331 multi-channel run.

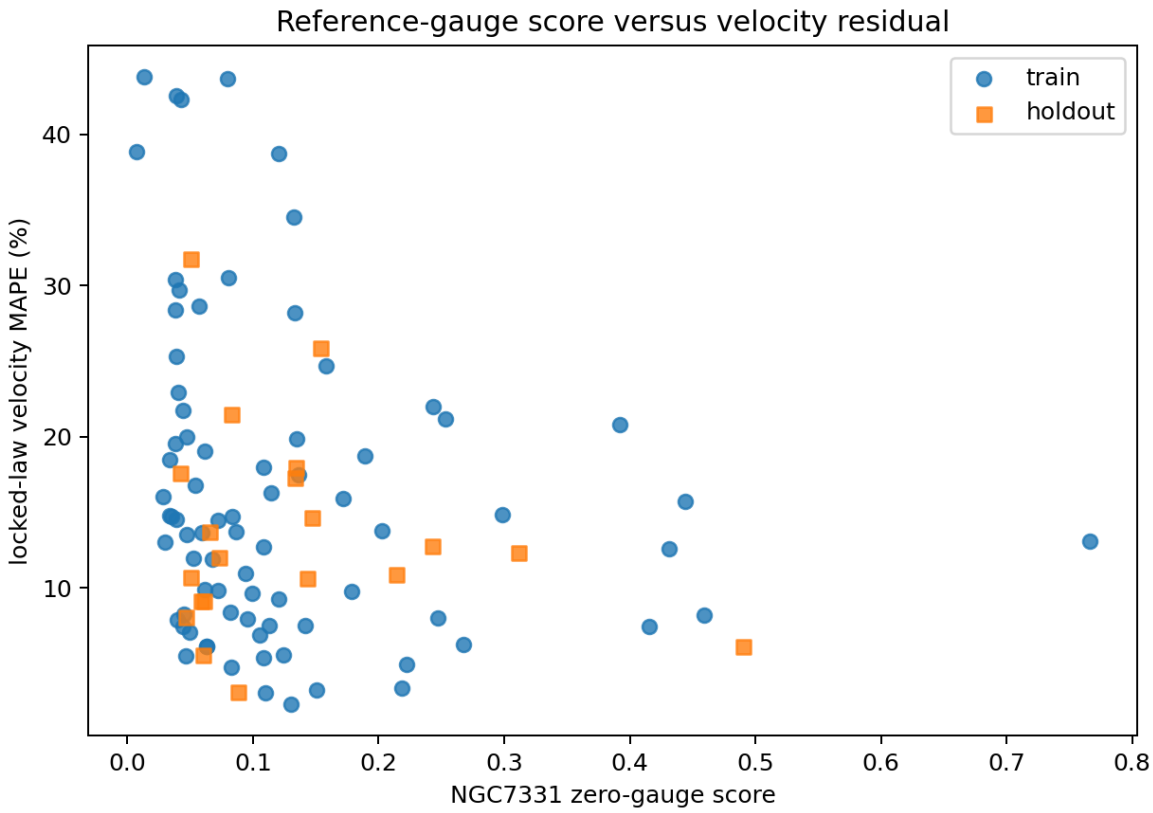

Figure 7: Zero-gauge score compared with locked-law velocity error. The gauge is a detector reference, not a velocity correction.

13.5 Feature importance

The improved detector leans most strongly on observed phase-gradient structure, observed phase strength, phase ratios, the event/lensing score, and the difference between forward and observed phase amplitudes. That pattern is consistent with the interpretation that the current remaining gap is switching and projection geometry rather than a new acceleration term.

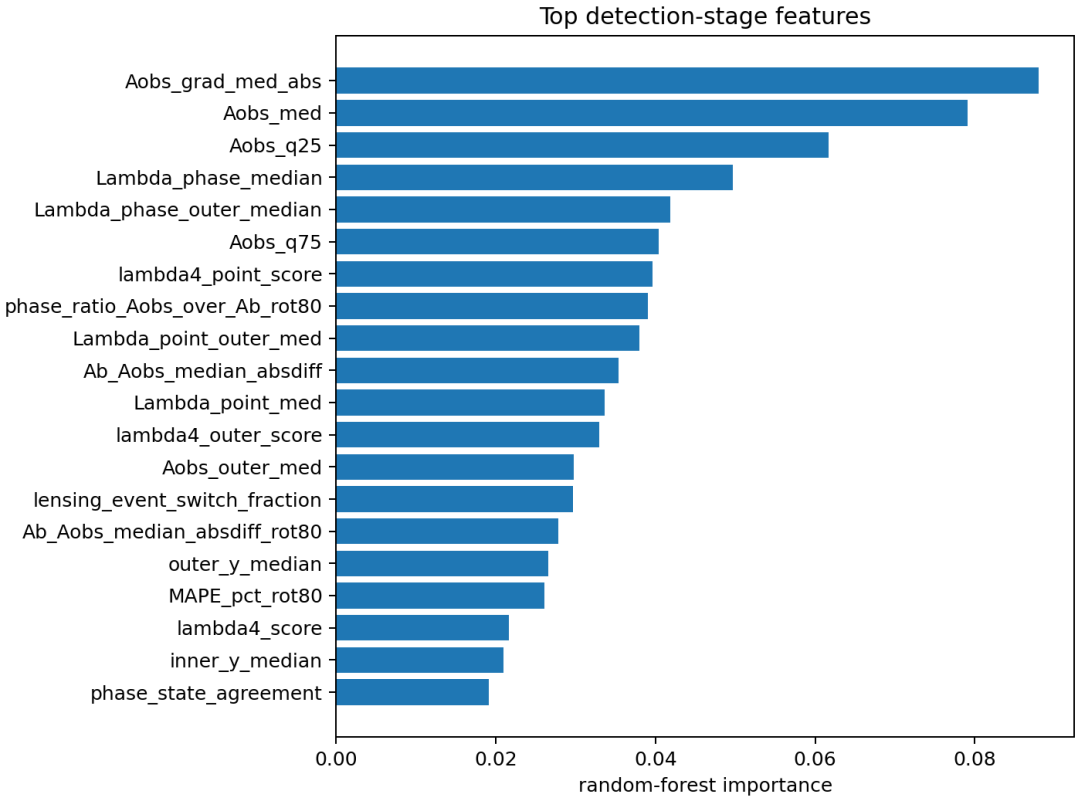

Figure 8: Top detector features in the NGC7331 multi-channel run.

Table 5: Top feature importances from the reference-gauge multi-channel detector.

Feature	Importance
Aobs_grad_med_abs	0.0881
Aobs_med	0.0791
Aobs_q25	0.0617
Lambda_phase_median	0.0497
Lambda_phase_outer_median	0.0419
Aobs_q75	0.0404
lambda4_point_score	0.0397
phase_ratio_Aobs_over_Ab_rot80	0.0391
Lambda_point_outer_med	0.0380
Ab_Aobs_median_absdiff	0.0354
Lambda_point_med	0.0336
lambda4_outer_score	0.0329
Aobs_outer_med	0.0298
lensing_event_switch_fraction	0.0296
Ab_Aobs_median_absdiff_rot80	0.0279

14 Lensing and Bullet proxy context

The event-band detector is motivated by lensing/event projection, but it does not use lensing as a force-law term. The package contains weak-lensing BTFR summaries, strong-lensing pilot correlations, and Bullet proxy outputs. It does not contain full raw arc images or observed κ pixels.

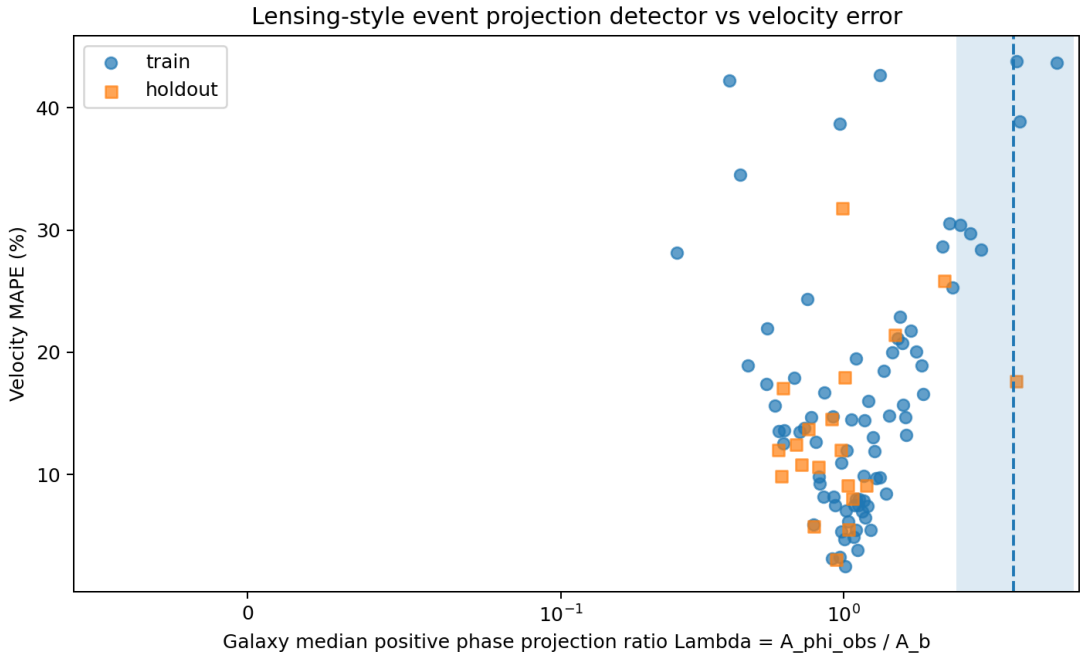

Figure 9: Projected phase ratio versus velocity error in the lensing detection-channel run. The projected ratio is a detector clue.

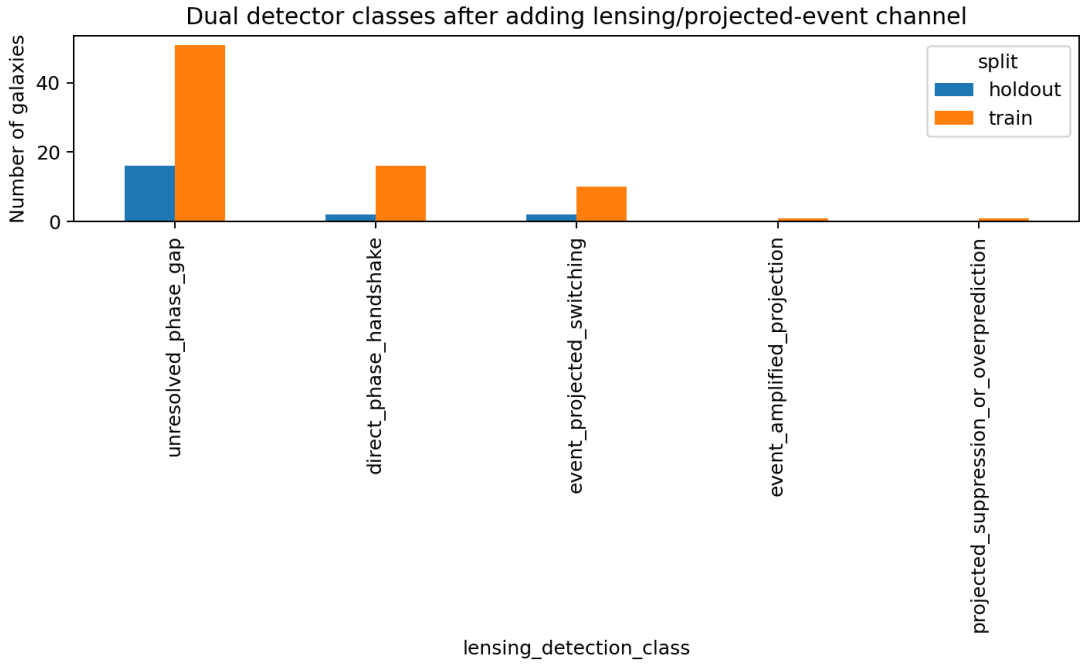

Figure 10: Lensing/event detection class counts. This is detection-stage classification only.

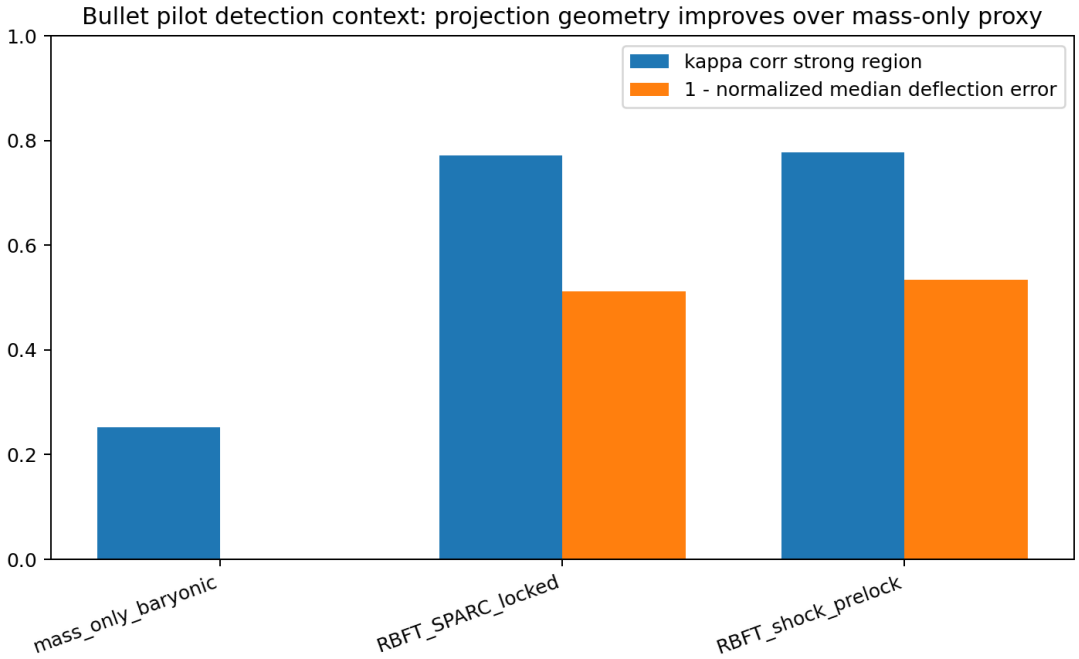

Figure 11: Bullet-style detection context. Event projection helps identify switching/amplified geometry but does not modify the locked law.

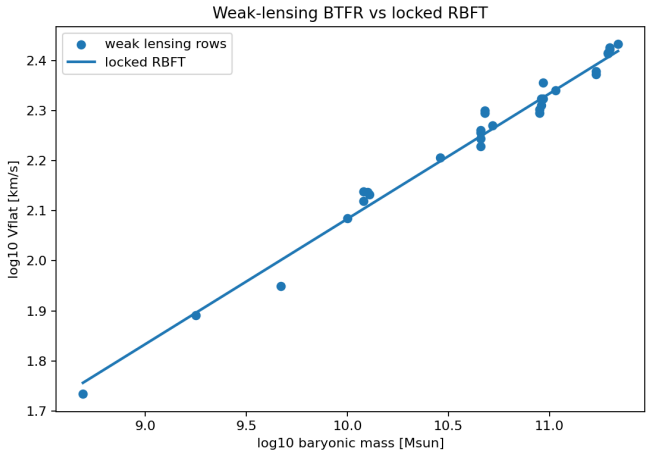

(a) Weak-lensing BTFR pilot.

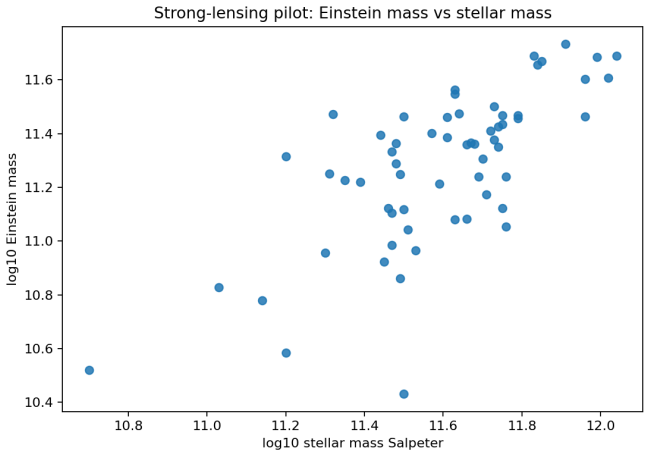

(b) Strong-lensing pilot.

Figure 12: Lensing pilot figures from the reproducibility package. These are pilot/proxy results, not full image-plane inversions.

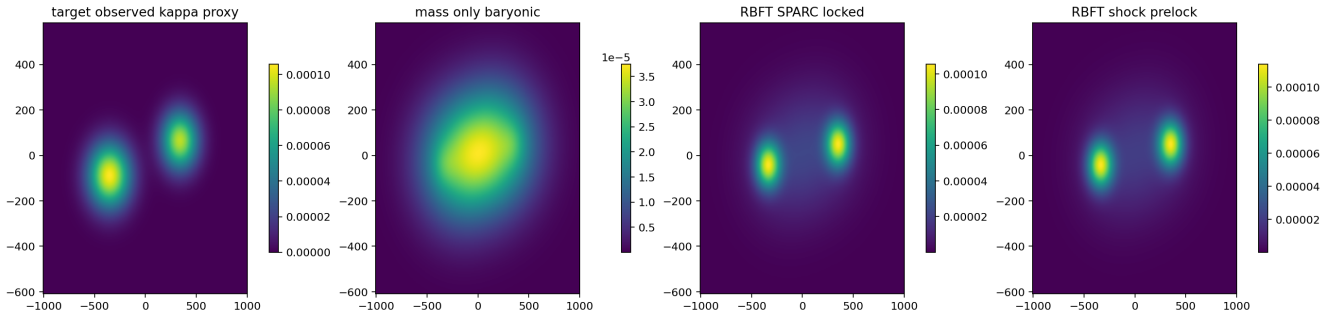

Figure 13: Bullet proxy maps. The proxy improves projected morphology relative to mass-only baryonic baselines, but full observed convergence-map fitting is still pending.

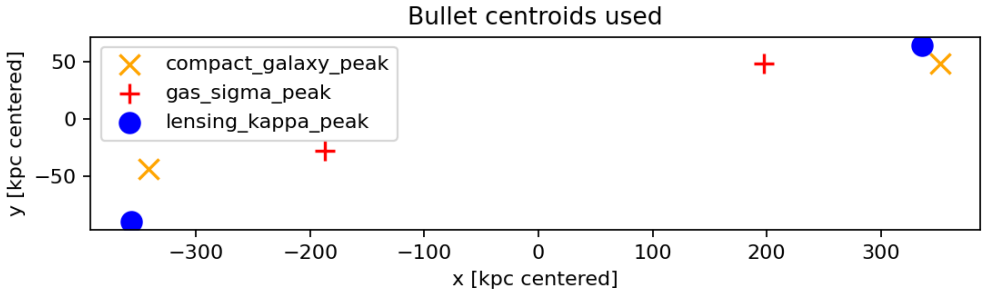

Figure 14: Bullet centroid offsets. This supports event/projection detection only; it is not treated as a locked-law correction.

15 How to reproduce the current result

An independent reader should be able to reproduce the present detector report as follows.

15.1 Data products

Use the supplied reproducibility package and output products:

- SPARC rotation and baryonic mass-model data from the RBFL SPARC reproducibility package.
- Locked-law prediction tables: galaxy-level MAPE and point-level predictions.
- Reference-gauge detector outputs: zero-gauge features, $A_{\phi,\mathrm{obs}}$ statistics, Λ statistics, state labels.
- Lensing/event-channel outputs: event projection candidate flags and lensing proxy summaries.
- Adjustable event-band output: `rbfl_lambda_band_detector_results.csv`, `lambda_band_split_summary.csv`, and `rbfl_lambda_band_sweep_results.csv`.

15.2 Step-by-step calculation

1. Compute the locked-law velocity prediction with Eq. (1). Record MAPE for every galaxy.
2. Compute observed detector variables only after the prediction exists: $A_{\phi,\mathrm{obs}}$, Φ, y, Λ, phase gradients, and state labels.
3. Set NGC7331 to $\theta = 0^\circ$ and compute relative gauge features.
4. Compute baryonic/geometric features: mass, gas fraction, compactness, R_d, z_d proxies, g_b, R_ϕ, and any rotation/drag proxy available from baryons.
5. For each event-band pair $(\lambda_{\mathrm{event}}, \sigma_\lambda)$, compute Q_λ.
6. Train a compact detector on training galaxies only, using the observed diagnostic state as the target label.
7. Freeze the detector and evaluate holdout galaxies.
8. Report phase match, velocity pass, combined pass, and the confusion table.

16 Interpretation of the latest result

The adjustable event-band result should be interpreted carefully.

- The detector improved from 75% to 95% holdout phase-state match.
- The locked-law velocity pass stayed at 70%, because no velocity prediction was altered.
- The combined velocity + phase tolerance improved from 60% to 70%.
- The improvement shows that projected event/switching geometry was present in the observables.
- The improvement is not a proof that the underlying law is complete; it is evidence that the detector can decode phase families better when event-projection information is included.

The practical conclusion is:

> The best current path is not to change the locked acceleration law. It is to improve phase detection, especially by acquiring true 3D data and more direct lensing/projection information.

17 Why more data matters

The detector now has enough observables to classify many phase states, but it is still approximating the 3D field from projections. The next improvements should come from:

- full 3D baryonic density reconstructions $\rho_b(R, \theta, z)$;
- gas maps, disk thickness, warps, bars, asymmetry, and central-node structure;
- actual lensing κ maps and source-plane arc inversions, not only proxy summaries;
- wide-binary 6D phase-space samples as local x, y, z tracers;
- independent timing/beat-envelope datasets if used;
- fresh held-out galaxy samples beyond the present SPARC split.

With those data, the detector should move from projected inference

$$A_b(r) \approx \mathcal{P}_r[A_b(\mathbf{x})] \tag{35}$$

toward direct field-shape reconstruction

$$A_b(\mathbf{x}) = A_b(R, \theta, z). \tag{36}$$

18 Symbol dictionary

Symbol	Definition
G	Newtonian gravitational constant.

Symbol	Definition
$\mathbf{x}$	Three-dimensional position vector.
r	Radial coordinate used for rotation-curve projection.
R, θ, z	Cylindrical disk coordinates.
$\rho_b(\mathbf{x})$	Three-dimensional baryonic density field.
$\Sigma_b(r)$	Projected baryonic surface density profile.
$M_b(< r)$	Enclosed baryonic mass within radius r.
$g_b(r)$	Newtonian baryonic acceleration.
$g_{\mathrm{RBFL}}(r)$	Locked RBFL radial acceleration prediction.
$\mathbf{g}_{\mathrm{RBFL}}(\mathbf{x})$	3D vector form of the RBFL acceleration prediction.
a_ϕ	Phase-carrier acceleration scale in the locked law.
a_Θ	Locked outer acceleration scale in $v_f^4 = GM_b a_\Theta$.
$A_b(\mathbf{x})$	Baryon-derived 3D phase-amplitude operator.
$A_b(r)$	Radial projection of the 3D phase operator.
$A_{\phi,\mathrm{obs}}(r)$	Residual-derived observed phase diagnostic, computed after observation.
A_{lock}	Locked-state reference amplitude.
S_{phase}	Phase strength from baryonic saturation.
D_{phase}	Phase degree/coherence from gradients and disk geometry.
H_{phase}	Height/envelope factor for 3D field reach.
G_{rot}	Central-node rotational geometry / drag factor.
B_{switch}	Boundary/switching detection factor.
Φ_{total}	Total local phase-field state.
Φ_{parent}	Parent saturated field.
Φ_b	Baryonic compression field.
Φ_{rot}	Rotation-organized phase field.
Φ_c	Critical phase scale for saturation.
$\Phi(r)$	Acceleration ratio detector, g_{obs}/g_b.
$y(r)$	Log detector, $\ln \Phi(r)$.
B_y	Radial phase drift statistic, outer log phase minus inner log phase.
$\theta_{\mathrm{NGC7331}}$	Zero-phase reference gauge, set to 0°.
Λ	Phase ratio, $A_{\phi,\mathrm{obs}}/A_b$.
λ_{event}	Detection-stage event/lensing band center. Not a law constant.
σ_λ	Event-band width.
Q_λ	Event-band detection score.
V_{pred}	Predicted circular speed from the locked law.
V_{obs}	Observed circular speed, used for scoring and post-test diagnostics.
MAPE	Median absolute percentage error in velocity.

19 Final record statement

The improved 3D Phase Field Prediction/Detection Unit keeps the RBFL acceleration law locked and moves all flexible interpretation into the detector. The detector estimates phase state from observable fingerprints. The present data lack full 3D baryonic and lensing information, so the detector uses projected observables and event/lensing bands to infer the field shape. In the latest run, this improved holdout phase-state

classification from 75% to 95%, while leaving the locked-law velocity pass unchanged at 70%. The result supports the idea that the main remaining work is detector refinement, especially with true 3D data, not changing the core law.

A Top event-band sweep rows

Table 7: First rows of the event-band sweep table.

Holdout phase	Combined	Train phase	Center	Sigma	Model
95.0%	70.0%	98.7%	2.0	0.25	rf3
95.0%	65.0%	94.9%	2.0	0.25	tree3
95.0%	70.0%	98.7%	2.0	0.40	rf3
95.0%	65.0%	94.9%	2.0	0.40	tree3
95.0%	70.0%	100.0%	2.0	0.55	rf3
95.0%	65.0%	94.9%	2.0	0.55	tree3
95.0%	70.0%	100.0%	2.0	0.70	rf3
95.0%	65.0%	94.9%	2.0	0.70	tree3
95.0%	70.0%	100.0%	2.5	0.25	rf3
95.0%	65.0%	94.9%	2.5	0.25	tree3
95.0%	70.0%	100.0%	2.5	0.40	rf3
95.0%	65.0%	94.9%	2.5	0.40	tree3
95.0%	70.0%	100.0%	2.5	0.55	rf3
95.0%	65.0%	94.9%	2.5	0.55	tree3
95.0%	70.0%	100.0%	2.5	0.70	rf3
95.0%	65.0%	94.9%	2.5	0.70	tree3

B Output package notes

The current PDF summarizes the following generated output families:

- `rbfl_lambda_event_band_test_outputs`: adjustable event-band detector results.
- `tmp_ref`: NGC7331 reference-gauge multi-channel detector outputs.
- `tmp_lens`: lensing/event detection-channel outputs.
- `tmp_bench`: benchmark suite outputs.

The reader can reproduce the numbers by loading the CSV files listed in these folders, using the equations and algorithm above, and verifying the reported split summaries.